Penn Libraries
UNIVERSITY OF PENNSYLVANIA

University of Pennsylvania
ScholarlyCommons

Departmental Papers (MSE)

Department of Materials Science & Engineering

8-4-2011

Diffusive Molecular Dynamics and its Application to Nanoindentation and Sintering

Ju Li
University of Pennsylvania; Xi' an Jiaotong University, liju@seas.upenn.edu

Sanket Sarkar
Ohio State University - Main Campus

William Cox
Ohio State University - Main Campus; Xi' an Jiaotong University

Thomas J. Lenosky
University of Pennsylvania

Erik Bitzek
University of Pennsylvania; Universität Erlangen-Nürnberg

See next page for additional authors

Follow this and additional works at: http://repository.upenn.edu/mse_papers

Part of the Materials Science and Engineering Commons

Recommended Citation

Diffusive Molecular Dynamics and its Application to Nanoindentation and Sintering

Abstract

The interplay between diffusional and displacive atomic movements is a key to understanding deformation mechanisms and microstructure evolution in solids. The ability to handle the diffusional time scale and the structural complexity in these problems poses a general challenge to atomistic modeling. We present here an approach called diffusive molecular dynamics (DMD), which can capture the diffusional time scale while maintaining atomic resolution, by coarse-graining over atomic vibrations and evolving a smooth site-probability representation. The model is applied to nanoindentation and sintering, where intimate coupling between diffusional creep, displacive dislocation nucleation, and grain rotation are observed.

Disciplines

Engineering | Materials Science and Engineering

Author(s)

Ju Li, Sanket Sarkar, William Cox, Thomas J. Lenosky, Erik Bitzek, and Yunzhi Wang

Diffusive molecular dynamics and its application to nanoindentation and sintering

Ju Li,[1,4,*] Sanket Sarkar,[2] William T. Cox,[2,4] Thomas J. Lenosky,[1] Erik Bitzek,[1,3] and Yunzhi Wang[2,4,†]

[1]*Department of Materials Science and Engineering, University of Pennsylvania, Philadelphia, Pennsylvania 19104, USA*
[2]*Department of Materials Science and Engineering, The Ohio State University, Columbus, Ohio 43210, USA*
[3]*Department Werkstoffwissenschaften, Universität Erlangen-Nürnberg, D-91058 Erlangen, Germany*
[4]*State Key Laboratory for Mechanical Behavior of Materials and Frontier Institute of Science and Technology, Xi'an Jiaotong University, Xi'an 710049, China*

The interplay between diffusional and displacive atomic movements is a key to understanding deformation mechanisms and microstructure evolution in solids. The ability to handle the diffusional time scale and the structural complexity in these problems poses a general challenge to atomistic modeling. We present here an approach called diffusive molecular dynamics (DMD), which can capture the diffusional time scale while maintaining atomic resolution, by coarse-graining over atomic vibrations and evolving a smooth site-probability representation. The model is applied to nanoindentation and sintering, where intimate coupling between diffusional creep, displacive dislocation nucleation, and grain rotation are observed.

I. INTRODUCTION

Materials' behavior depends on processes that take place on a variety of time scales. These range from atomic vibrations or dislocation-mediated slip processes, which have typical time scales of hundreds of femtoseconds (fs) to hundreds of picoseconds (ps), to diffusion, which may take place on the order of seconds or longer. This disparity in time scales leads to difficulties when trying to model slower processes where individual atomic motions may be important, such as diffusion controlled boundary migration and dislocation climb. A straightforward molecular dynamics (MD) approach, with a typical time step of 1fs, would require an enormous computation time to adequately capture these processes. This has lead to the development of a variety of techniques to overcome the time scale limitations of MD. Phase-field crystal methods[1] coarse-grain over atomic vibrations to achieve longer time scale, but the use of a plane-wave basis restricts its applications. Transition state theory (TST) based approaches such as hyper-MD[2,3] suffer from the problem of low barriers. Also, representing long-ranged diffusion by instantiating billions of vacancy random walks individually at TST level is often neither practical nor necessary. Kinetic Monte Carlo (KMC) methods use a catalog of possible events, but a complete catalog may be difficult to create for complex systems. On-the-fly KMC,[4] in principle, circumvents this problem by building a state-specific catalog on the fly, but programming and computational overheads are very demanding. In this paper we present a chemical and kinetic extension of the variational Gaussian (VG) method,[5,6] called diffusive molecular dynamics (DMD), to model coupled diffusional-displacive processes.[7]

II. METHODOLOGY

A. Theory

In traditional MD, $6N$ variables, the atomic positions and momenta $\{\mathbf{x}_i, \mathbf{p}_i\}, i = 1 \ldots N$, where N is the number of atoms, are numerically integrated. However, most atomic motions in solids are spent in thermal vibrations about some mean position $\mathbf{X}_i \equiv \langle \mathbf{x}_i \rangle$. When viewed on time scales much longer than the vibrational, an atom appears as a density cloud. In most solids, the extent of these vibrations is narrow enough and nearly isotropic such that one atomic density cloud can be approximated by a normalized Gaussian

$$G(\mathbf{x}_i|\mathbf{X}_i, \alpha_i) = (\alpha_i/\pi)^{d/2} \exp[-\alpha_i|\mathbf{x}_i - \mathbf{X}_i|^2], \quad (1)$$

where α_i is related to the Debye-Waller factor, $\alpha_i = m_i \omega_i^2 / 2k_B T$ if in the Einstein model solid, m_i is the atomic mass, ω_i is the Einstein frequency and d is the dimensionality of the system, k_B is the Boltzmann constant, and T is the absolute temperature.

In real systems, atomic vibrations are correlated with those of nearby atoms. If the correlation effect is small, the Gibbs-Bogoliubov inequality to a reference system of Einstein oscillators may yield a variational upper bound F_{VG} that well approximates the real Helmholtz free energy.[5] For an embedded atom method (EAM) potential, this gives[6]

$$F_{VG} = \frac{1}{2} \sum_{i=1}^{N} \sum_{j \neq i} w(X_{ij}, \alpha_{ij}) + \sum_{i=1}^{N} E(\overline{\psi}_{i,VG})$$
$$+ \frac{d}{2} k_B T \sum_{i=1}^{N} \left\{ \ln\left[\frac{\alpha_i \Lambda_T^2}{\pi}\right] - 1 \right\}, \quad (2)$$

where $\overline{\psi}_{i,VG} = \sum_{j \neq i} \psi(X_{ij}, \alpha_{ij})$, $\Lambda_T = \hbar\sqrt{2\pi/m_i k_B T}$ is the de Broglie thermal wavelength, $X_{ij} = |\mathbf{X}_i - \mathbf{X}_j|$, $\alpha_{ij} \equiv (\alpha_i^{-1} + \alpha_j^{-1})^{-1}$, E is the EAM embedding function, w is the Gaussian-averaged pair potential u, and ψ is the Gaussian-averaged density function ρ of the EAM potential (discussed in detail later). Here, the ensemble average of the embedding function ($\langle E \rangle_0$) has been approximated by averaging the Taylor expansion of the embedding energy and dropping second- and higher-order moments. Though the second moment is small and positive (0.001 eV/atom in Cu[6]), the final free energy is no longer guaranteed to be an absolute upper bound. In the VG method, F_{VG} is minimized with respect to $\{\mathbf{X}_i, \alpha_i\}$ to estimate the real Helmholtz free energy. This method has $4N$ degrees of freedom (Gaussian width and mean position) in contrast to the $6N$ variables of traditional MD, and requires

only static minimization. LeSar et al.[6] have tested the accuracy of VG method by comparing it with an exact free-energy calculation of Foiles and Adams using EAM over a wide range of temperatures.[8]

To extend this model to handle diffusive mass transport by vacancy exchange, for instance, one could consider a Monte Carlo VG (MCVG) simulation in which one would swap empty sites with adjacent occupied sites, relax $\{\mathbf{X}_i, \alpha_i\}$, and then accept or reject the swap. But there is a considerable computational cost from many such random swaps with relaxation. A much faster method is to consider the ensemble average where each site, instead of being either vacant or occupied, has a continuous occupation probability $c_i \in (0,1)$, where $c_i = 0$ resembles a site vacancy with complete certainty, and $c_i = 1$ resembles an atom (say Cu) with complete certainty. In multicomponent alloys, c_i is generalized from a scalar to a vector to represent site chemical composition, and using such site "color" and density cloud is philosophically akin to the Kohn-Sham density functional theory (DFT) for electrons.[9] A variational Helmholtz free energy that incorporates these site "colors" can be derived by applying the Gibbs-Bogoliubov inequality to a reference system of harmonic oscillators in the grand canonical ensemble, which yields

$$
\begin{aligned}
F_{\mathrm{DMD}} = {} & \frac{1}{2} \sum_{i=1}^{N} \sum_{j \neq i} c_i c_j w(X_{ij}, \alpha_{ij}) + \sum_{i=1}^{N} c_i E(\overline{\psi}_i) \\
& + \frac{d}{2} k_{\mathrm{B}} T \sum_{i=1}^{N} c_i \left\{ \ln \left[\frac{\alpha_i \Lambda_T^2}{\pi} \right] - 1 \right\} \\
& + k_{\mathrm{B}} T \sum_{i=1}^{N} \{ c_i \ln c_i + (1 - c_i) \ln(1 - c_i) \},
\end{aligned}
\tag{3}
$$

where

$$
\overline{\psi}_i = \sum_{j \neq i} c_j \psi(X_{ij}, \alpha_{ij}). \tag{4}
$$

We may define an exchange chemical potential between an atom and a vacancy for site i by differentiating Eq. (3),

$$
\mu_i \equiv \frac{\partial F_{\mathrm{DMD}}(\{\mathbf{X}_i, \alpha_i, c_i\})}{\partial c_i}, \tag{5}
$$

and identify an exchange formation energy

$$
f_i \equiv \mu_i - k_{\mathrm{B}} T \ln \left[\frac{c_i}{1 - c_i} \right] \tag{6}
$$

which excludes the configurational entropy contribution.

Following the master equation, the rate of change of the site probability is given by

$$
\begin{aligned}
\frac{dc_i}{dt} = \sum_{j}{}' & \nu \exp \left[-\frac{Q_{\mathrm{m}}}{k_{\mathrm{B}} T} \right] \left\{ c_j (1 - c_i) \exp \left[-\frac{f_{ij}}{2 k_{\mathrm{B}} T} \right] \right. \\
& \left. - c_i (1 - c_j) \exp \left[\frac{f_{ij}}{2 k_{\mathrm{B}} T} \right] \right\},
\end{aligned}
\tag{7}
$$

where the primed summation is over diffusing neighbors, currently taken to be the first nearest neighbors. The steric factors $c_j(1 - c_i)$, $c_i(1 - c_j)$ reflect the observation that diffusional jumps can only happen if one site is occupied while the other site is empty: If both sites are fully empty or fully occupied, then mass exchange cannot happen kinematically. ν is the jump attempt frequency, and $Q_{\mathrm{m}} = F_{ij}^* - (f_i + f_j)/2$ is the activation energy for vacancy migration, where F_{ij}^* is the saddle height energy between site i and j. $f_{ij} \equiv f_i - f_j$ is the difference in formation energies between the two sites. For simplicity, in the current implementation the vacancy migration attempt frequency ν and activation energy Q_{m} are assumed to be independent of a site's local structural and chemical environment, i.e., the spatial arrangements of nearby sites. But in principle, one could develop and then use environment-dependent ν and Q_{m} functions in DMD simulations, which have been previously parametrized against experimentally measured or DFT-computed diffusivities. For example, one may develop a local diffusivity expression that varies with the coordination number and that is fitted to a database of bulk, surface, dislocation core, and grain boundary diffusivities. In the current implementation, by linearizing Eq. (7), one can estimate the vacancy diffusivity D_{V} as

$$
D_{\mathrm{V}} = \frac{Z}{2d} \nu b^2 \exp \left[-\frac{Q_{\mathrm{m}}}{k_{\mathrm{B}} T} \right], \tag{8}
$$

where b is the nearest-neighbor distance, and Z is the coordination number. Because displacive relaxation of $\{\mathbf{X}_i, \alpha_i\}$ is "instantaneous" in DMD, the fundamental "clock" of DMD is controlled by the value of chemical diffusivity, not by atomic vibration. We thus define

$$
\tilde{t} \equiv \frac{4 \pi D_{\mathrm{V}} t}{b^2} \equiv \frac{t}{\tau} \tag{9}
$$

to be the dimensionless (reduced) time.

Equation (7) satisfies mass conservation since the pair mass-exchange rate $c_j(1 - c_i) \exp[-f_{ij}/2k_{\mathrm{B}}T] - c_i(1 - c_j) \exp[f_{ij}/2k_{\mathrm{B}}T]$ is antisymmetric with respect to $i \leftrightarrow j$ permutation. One can also prove that F_{DMD} will decay monotonically with time, since

$$
\begin{aligned}
(\mu_i - \mu_j) & \left\{ c_j(1 - c_i) \exp \left[-\frac{f_{ij}}{2 k_{\mathrm{B}} T} \right] - c_i(1 - c_j) \exp \left[\frac{f_{ij}}{2 k_{\mathrm{B}} T} \right] \right\} \\
& = \left(f_{ij} + k_{\mathrm{B}} T \ln \frac{c_i(1 - c_j)}{(1 - c_i)c_j} \right) \left\{ c_j(1 - c_i) \exp \left[-\frac{f_{ij}}{2 k_{\mathrm{B}} T} \right] - c_i(1 - c_j) \exp \left[\frac{f_{ij}}{2 k_{\mathrm{B}} T} \right] \right\}
\end{aligned}
\tag{10}
$$

is nonpositive, contributing to chemical dissipation in the system.

B. Implementation

DMD has $5N$ degrees of freedom $\{\mathbf{X}_i, \alpha_i, c_i\}$, which are the mean position, Gaussian width, and the occupation probability of site density clouds, in contrast to the $6N$ variables of traditional MD. During a DMD simulation, each time step is realized in two parts. First, the variables $\{\mathbf{X}_i, \alpha_i\}$ are statically minimized as in the VG method, while holding $\{c_i\}$ constant. This process can be assumed to take place instantaneously because $\{\mathbf{X}_i\}$ and $\{\alpha_i\}$ change on the inertial (ps) and thermalization (100 ps) time scales, respectively, both of which are much smaller than τ. Then in the second part, the $\{c_i\}$ are integrated numerically according to Eq. (7) while holding $\{\mathbf{X}_i, \alpha_i\}$ constant. This is equivalent to assuming that the system is always in vibrational and mechanical equilibrium, but not chemical equilibrium, at each time step. It is therefore not possible to model dynamical effects where inertia plays a role.

In the simulations below for pure Cu, we use the Mishin EAM potential.[10] The Gaussian averaged pair potential $w(X_{ij}, \alpha_i, \alpha_j)$ and the Gaussian averaged electron density function $\psi(X_{ij}, \alpha_i, \alpha_j)$ are originally given as[6]

$$
\begin{aligned}
w(X_{ij}, \alpha_i, \alpha_j) &= \left(\frac{\alpha_i}{\pi}\right)^{d/2} \left(\frac{\alpha_j}{\pi}\right)^{d/2} \int \cdots \int d\mathbf{x}_i d\mathbf{x}_j \\
&\quad \times e^{-\alpha_i(\mathbf{x}_i - \mathbf{X}_i)^2} e^{-\alpha_j(\mathbf{x}_j - \mathbf{X}_j)^2} u(x_{ij}), \\
\psi(X_{ij}, \alpha_i, \alpha_j) &= \left(\frac{\alpha_i}{\pi}\right)^{d/2} \left(\frac{\alpha_j}{\pi}\right)^{d/2} \int \cdots \int d\mathbf{x}_i d\mathbf{x}_j \\
&\quad \times e^{-\alpha_i(\mathbf{x}_i - \mathbf{X}_i)^2} e^{-\alpha_j(\mathbf{x}_j - \mathbf{X}_j)^2} \rho(x_{ij}),
\end{aligned}
\tag{11}
$$

where $\mathbf{x}_{ij} = \mathbf{x}_i - \mathbf{x}_j$, $x_{ij} = |\mathbf{x}_{ij}|$, and $u(x)$ and $\rho(x)$ are the pair potential and the electron density function of the EAM potential, respectively. In the VG method, LeSar et $al.$[6] fitted the functions w and ψ to a sum of Gaussian functions of the interatomic distance. For the present study, w and ψ were numerically integrated to create a 2-dimensional lookup table which was then used with bicubic interpolation to achieve a better accuracy. The procedure is described below.

It can be proven using Fourier transform that if two particles are independently Gaussian, then their separation vector $\mathbf{x}_{ij}$ is also a Gaussian cloud with parameter

$$
\alpha_{ij} = \left(\alpha_i^{-1} + \alpha_j^{-1}\right)^{-1}.
\tag{12}
$$

If there is an offset $\mathbf{X}_{ij}$ in the centers of the two clouds, then the above Gaussian is also shifted by $\mathbf{X}_{ij}$. Therefore Eq. (11) can be rewritten in the form of

$$
\begin{aligned}
w(X_{ij}, \alpha_{ij}) &= \left(\frac{\alpha_{ij}}{\pi}\right)^{d/2} \int \cdots \int d\mathbf{x}_{ij} e^{-\alpha_{ij}(\mathbf{x}_{ij} - \mathbf{X}_{ij})^2} u(|\mathbf{x}_{ij}|), \\
\psi(X_{ij}, \alpha_{ij}) &= \left(\frac{\alpha_{ij}}{\pi}\right)^{d/2} \int \cdots \int d\mathbf{x}_{ij} e^{-\alpha_{ij}(\mathbf{x}_{ij} - \mathbf{X}_{ij})^2} \rho(|\mathbf{x}_{ij}|).
\end{aligned}
\tag{13}
$$

Furthermore, for integration, one can choose a coordinate system in which the origin is identical to the origin of the effective Gaussian. Then, in 3D, the Gaussian averaged potential and density function become

$$
\begin{aligned}
w(X, \alpha) &= 2\pi \left(\frac{\alpha}{\pi}\right)^{3/2} \int_0^{r_c} \int_0^\pi r^2 dr d\theta \sin\theta \\
&\quad \times u(\sqrt{r^2 + X^2 + 2rX\cos\theta}) \exp[-\alpha r^2], \\
\psi(X, \alpha) &= 2\pi \left(\frac{\alpha}{\pi}\right)^{3/2} \int_0^{r_c} \int_0^\pi r^2 dr d\theta \sin\theta \\
&\quad \times \rho(\sqrt{r^2 + X^2 + 2rX\cos\theta}) \exp[-\alpha r^2],
\end{aligned}
\tag{14}
$$

where r_c is the cutoff on the Gaussian. Since the integrand in both cases is the product of a Gaussian and u or ρ, the cutoff in X for w and ψ is the sum of r_c and the cutoff of the respective functions. For Cu EAM potential[10] the cutoff is after 5.5 Å in both the pair potential and density function. The choice of r_c is a compromise between accuracy and efficiency since longer cutoffs will better match the integrals in Eq. (13) but include more atoms in the calculations during simulations. The 2-dimensional lookup tables used in the current implementation of the DMD method cut the Gaussian off after 1 Å. Experience has shown that producing a table for α from $10 \, \text{Å}^{-2}$ to $210 \, \text{Å}^{-2}$ is adequate for simulations run at temperatures of 500 K or higher using either the Morse potential used in the original VG work[5] or Cu EAM potential.[10] For $r_c = 1$ Å, this integration includes 4 standard deviations of the widest Gaussian of the table $\alpha = 10 \, \text{Å}^{-2}$ while adding 2 neighbor shells to calculations.

For the calculation of mechanical stress tensor, with $\{\alpha_i\}$ instantaneously minimized for arbitrary $\{\mathbf{X}_i, c_i\}$ configuration, it can be shown that the virial stress formula can be applied to just the first two terms of Eq. (3) to calculate the stress tensor in DMD, as if it were the normal interatomic potential in MD with $\mathbf{X}_i$ replaced by $\mathbf{x}_i$, and pretending $\{\alpha_i, c_i\}$ are frozen parameters.

The displacive relaxation step in DMD was implemented with L-BFGS,[11] a limited memory quasi-Newton optimization algorithm, and the chemical integration step with CVODE, a solver for stiff and nonstiff initial value problems for systems of ordinary differential equation from SUNDIALS.[12] Otherwise, the programmatic structure of DMD is identical to that of MD, which means lightweight code patches can be easily applied onto a MD code base. We have accomplished this successfully on LAMMPS,[13,30] taking advantage of its efficient parallelism for short-range interactions. It should be obvious from the formulation above that as $T \to 0$ and diffusion kinetics are frozen, DMD/VG will give identical results as $T \to 0$ classical MD. This is shown in Table I, where the DMD free energy,

TABLE I. Comparison of lattice parameter a_0, (free) energy per atom F_{DMD}/atom, bulk modulus K, and vacancy formation (free) energy E_V^f of the Gaussian averaged potential at 1K with Mishin EAM potential (Ref. 10) for Cu at 0K. Calculations were performed with $(1 - c) = 10^{-20}$ on occupied sites and $c = 10^{-20}$ on vacant sites.

	a_0 (Å)	F_{DMD} (eV/atom)	K (GPa)	E_V^f (eV)
Original EAM (0K)	3.615	-3.54	138.3	1.272
Gaussian averaged potential (1K)	3.621	-3.53	136	1.277

(a)   (b)   (c)
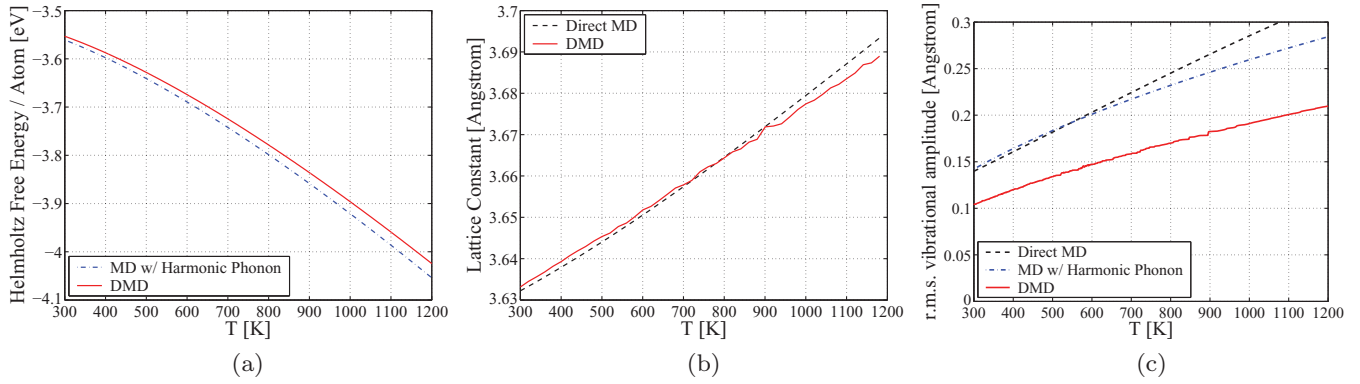
FIG. 1. (Color online) Benchmarking VG/DMD with Mishin EAM potential (Ref. 10) for Cu. Calculations were performed with $(1 - c) = 10^{-20}$ on occupied sites of a perfect crystal. (a) Helmholtz free energy per atom F_{DMD}/atom (red solid line), in comparison with analytical free energy $e_0 + N^{-1} \sum_{k=1}^{3N} k_B T \ln(\hbar\omega_k/k_B T)$ based on harmonic phonon theory (blue dash-dotted line), with phonon frequencies $\{\omega_k\}$ extracted from $T \approx 0$ MD simulations. (b) Lattice parameter a_0 from DMD calculation (red solid line), in comparison with direct MD simulations (black dashed line). (c) Root mean square displacement $(\langle|\mathbf{x}_i - \mathbf{X}_i|^2\rangle)^{1/2}$ per atom, based on DMD calculation $(=[3(2\alpha)^{-1}]^{1/2}$, red solid line), full-spectrum harmonic phonon theory $(=[N^{-1} \sum_{k=1}^{3N} k_B T (m\omega_k^2)^{-1}]^{1/2}$, blue dash-dotted line), and direct MD simulations (black dashed line).

elastic properties, lattice parameter, and vacancy formation energy as $T \to 0$ are seen to be all in excellent agreement with direct MD, using the same EAM potential[10] for Cu.

Next we check some finite-temperature properties against MD, in Fig. 1. We see that the thermal expansion and zero-pressure free energy are in excellent agreement with direct MD calculation and full-spectrum harmonic phonon theory, respectively, giving us confidence that VG can provide reasonable finite-temperature properties up to 90% of the melting point. However, the root mean squared displacements in the VG representation is about 30% *lower* than the actual value from direct MD. Philosophically, the reason for the simultaneously good agreements in Figs. 1(a) and 1(b) but not-so-good agreement in Fig. 1(c) has more to do with the VG *representation*, and less to do with the VG *formulation*. Just as in Kohn-Sham DFT for electrons where one maps an actual interacting-electrons system to a hypothetical system of noninteracting electrons,[9] VG maps an interacting-atoms system onto a noninteracting-atoms Einstein solid. When the motions of nearby atoms are uncorrelated as in an Einstein solid, the vibrational amplitude has to be smaller to prevent two neighboring atoms from getting too close to each other. On the other hand, in an interacting-atoms solid the oscillations are correlated, so both atoms could oscillate in the same direction, increasing the root mean squared displacement for a single atom without incurring a huge energy penalty for getting too close to each other, e.g., forming a "correlation hole" in the 2-particle distance distribution. This deficiency in geometrical representation does not seem to prevent VG from giving reasonable vibrational free energy and thermal expansion, though.

Presently, the site density clouds stay spherical even when the crystal is sheared, or near low-symmetry defects like surfaces. A straightforward improvement is to introduce anisotropic or even non-ellipsoidal density clouds, by variationally tuning the model potential *shapes* in the Einstein reference solid. This, however, will introduce additional complexities in the Eqs. (11)–(14) effective potentials.
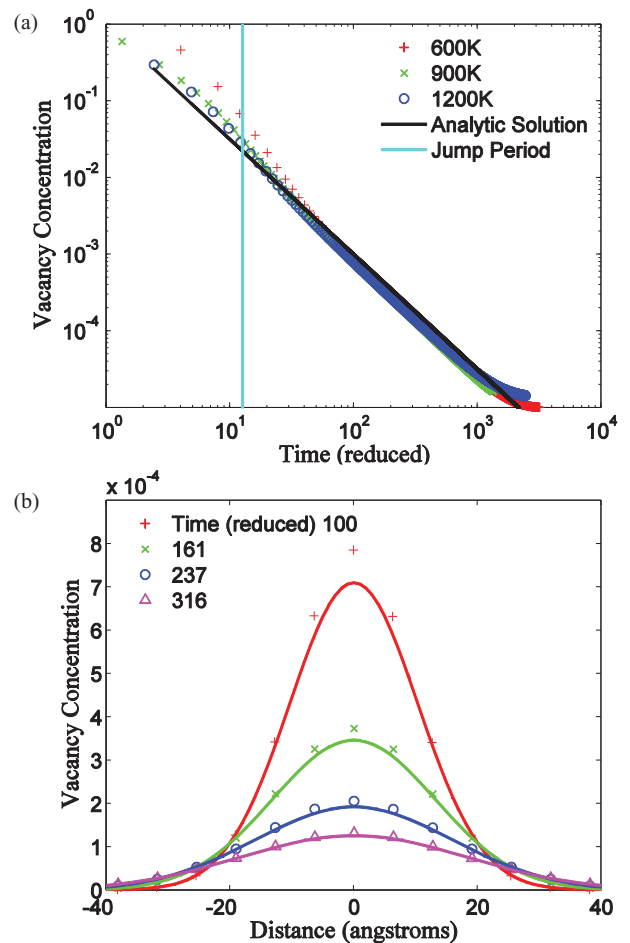

(a)

(b)

FIG. 2. (Color online) (a) Vacancy concentration of the initially vacant site over time at several temperatures. Lines show the analytic solution and mean vacancy jump period b^2/D_V. (b) Vacancy concentration along the [111] direction for different reduced times at 900 K. Solid lines show the analytic solutions.
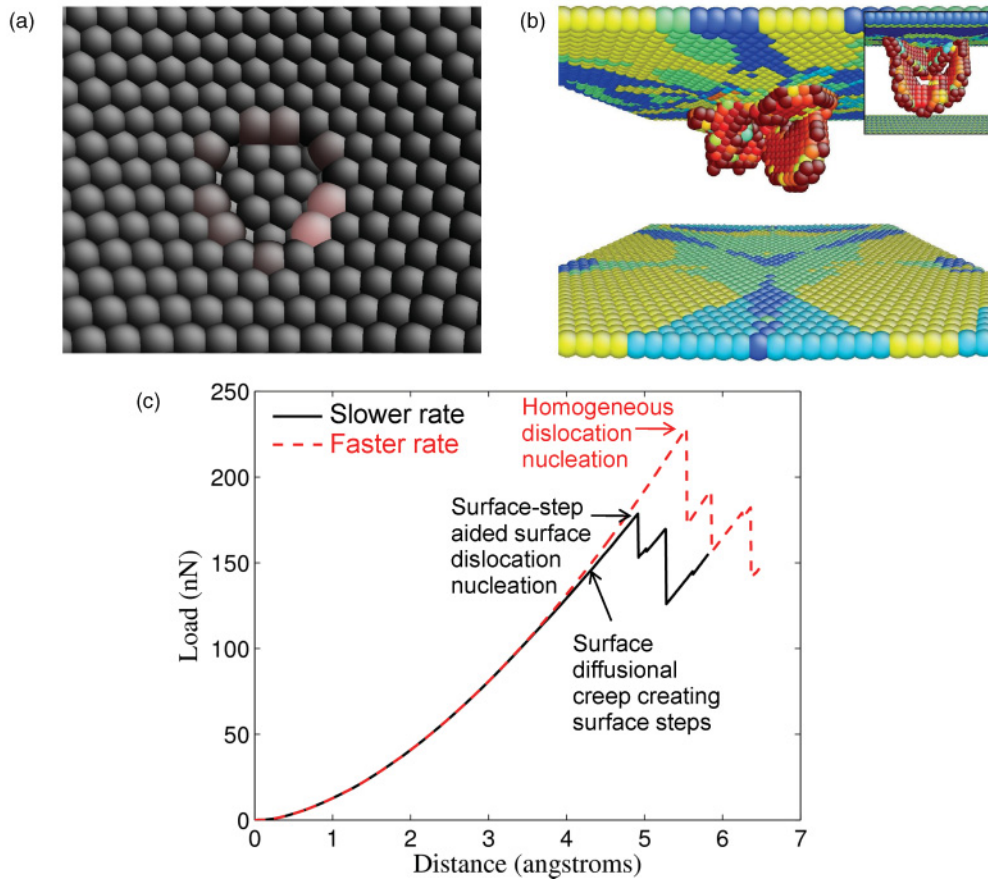
FIG. 3. (Color online) (a) Indenter accommodation by pure diffusional creep in the form of a surface vacancy disk at $\tilde{t} = 1000$ for the slower indentation rate. The black to white color scale represents the value of c with black signifying fully occupied sites. Atomic sites having $c \leqslant 0.01$ are not shown. (b) Dislocation structures viewed by centrosymmetry parameter (Ref. 21) along $[11\bar{2}]$ direction. Dislocation nucleation occurs at $\tilde{t} = 1010$. In the inset, shown is a typical dislocation loop grown after homogeneous nucleation. (c) Load-displacement curve for slower and faster rate indentation showing reduced dislocation nucleation load, due to surface vacancy disk/terrace created by prior diffusion.

For ease of checking, the source code of DMD and input files for all examples in this paper will be placed at a publicly available website.[30]

C. Validation

Before performing DMD simulations, the model is validated against the analytical random-walker solution of vacancy diffusion by examining diffusion of a single vacancy under periodic boundary conditions (PBC). Imagine one instantiates a vacancy in an otherwise perfect crystal, and then allows diffusive jumps to happen, by for instance performing Monte Carlo VG (MCVG) simulations. After many jump periods, the vacancy concentrations on various sites are expected to follow the analytical solution of the diffusion equation for a point source,[14] also known as the random-walker solution. In particular, the vacancy concentration for a site at a distance ΔX from the initial vacancy at time t is given by

$$c_V(\Delta X, \tilde{t}) \approx \Omega(\tilde{t}b^2)^{-d/2} \exp[-\pi \Delta X^2/(\tilde{t}b^2)], \quad (15)$$

where Ω is the average atomic volume, and $\tilde{t} = 4\pi D_V t/b^2$ is the dimensionless reduced time, b being the nearest neighbor distance. A simulation cell spanned by the fcc lattice vectors

$30 \times [100], 30 \times [010]$, and $30 \times [001]$ (consisting of 108000 sites) was chosen with one site being vacant ($c = 10^{-20}$). All the occupied sites were initially assigned the equilibrium vacancy concentration of $c_V^{Eq} = \exp(-E_V^f/k_B T)$ with $E_V^f = 1.25$ eV and a value of α corresponding to that of an atom in a bulk crystal at the temperature of interest. We chose $Q_m = 0.7$ eV and $\nu = 1 \times 10^{13}$ s^{-1} to match the experimental bulk vacancy diffusivity D_V^{bulk} of Cu. Figure 2 shows the simulation results, which match the analytical solution well with $d = 3$ and significant deviation occurring only at times shorter than the mean jump period and at long times when the system begins interacting with its images under PBC. This deviation at short times is expected as the Gaussian point-source solution[14] is the result of solving a continuum partial differential equation, valid in the limit when an infinite number of random walks have been executed, whereas DMD gives solution to the master equation when only a finite number of random walks has been executed on a discrete lattice.

III. RESULTS

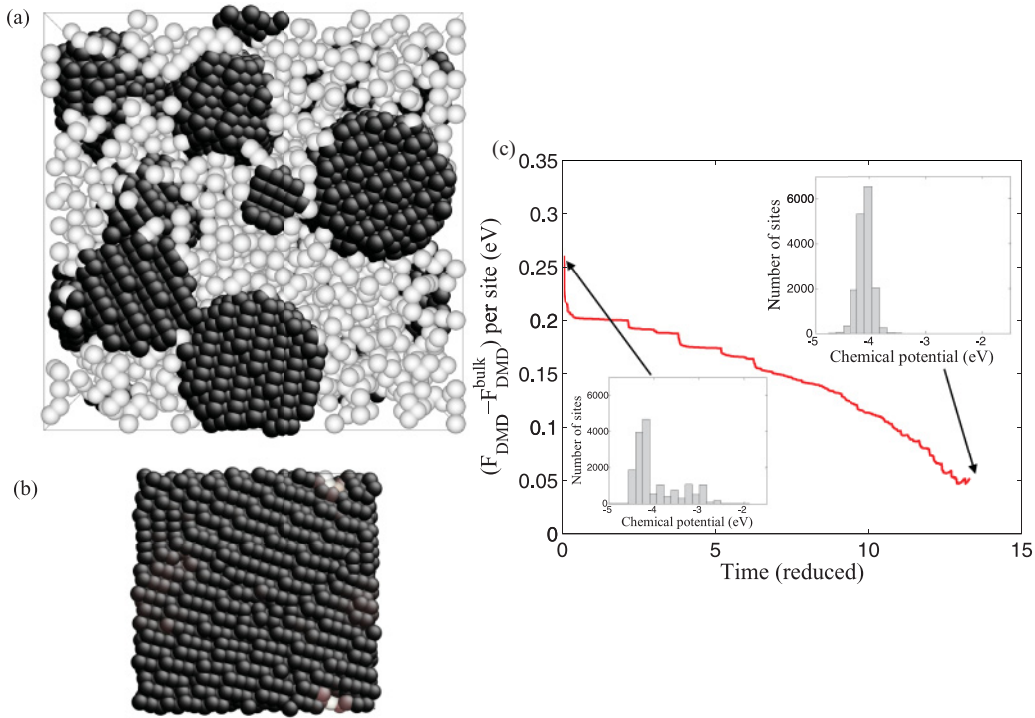We chose examples of nanoindentation and hot isostatic pressing of pure copper to demonstrate the capabilities of

FIG. 4. (Color online) (a) Initial configuration with $c = 0.9999$ for black sites, $c = 0.0001$ for white sites. (b) Final configuration after compressing to theoretical density over a reduced time of $\tilde{t} = 13.30$. Atomic sites with $c \leqslant 0.01$ are not shown. A movie of this simulation is included in the supplementary online material (Ref. 25). (c) Time evolution of F_{DMD} per site referenced to the bulk free energy $F_{\text{DMD}}^{\text{bulk}}$ per site for a perfect crystal. In the inset, distribution of site-wise chemical potential is shown for the initial and final configurations.

DMD in resolving coupled diffusive and displacive atomic movements.[7] At 900 K, though our model predicts an equilibrium vacancy concentration of 10^{-7}, a higher background vacancy concentration of 10^{-4} was used by assigning $c = 0.9999$, unless otherwise specified. The reason for this is that with $(1 - c) \approx 10^{-7}$ (the entire system has less than one vacancy typically), one needs to choose a stricter tolerance in solution vector $\{c_i\}$, preventing the solver from reaching the time scale necessary for transporting required vacancies from far field in reasonable computation time. Such nonequilibrium vacancy concentration can actually be found in many physical situations, such as irradiation damage, Kirkendall effect, and severe plastic deformation during cold rolling and fatigue.[15,16] In the bulk, the diffusivity was set to D_V^{bulk} as in the random-walker validation. Due to the importance of surface diffusion in nanoindentation and sintering, higher diffusivity was attributed to the surface sites using a simple scheme where the diffusivity was increased to $D_V^S = \chi D_V^{\text{bulk}}, \chi \geqslant 1$, if the weighted coordination ($\sum_j' c_j$) of diffusing sites is less than $Z - 1$. We chose χ to be 1000 since grain boundary and surface diffusivity values are typically three orders of magnitude higher than that of the bulk. The definition of reduced time $\tilde{t}$, however, was not modified.

A. Nanoindentation

In nanoindentation, different mechanisms can contribute to the total plastic strain. At low indentation rates or high temperatures, diffusional creep may occur due to the chemical potential gradient produced by stress field beneath the indenter.

This accommodates the indenter by diffusing surface layers of atoms away from the contact area, forming recessed terraces.[17] Further building-up of strain, however, leads to nucleation of gliding dislocations. To study these mechanisms, a frictionless spherical indenter with a radius of 40 Å was pressed onto a Cu(111) surface at 900 K at two different rates of 4.89×10^{-3} Å/τ, henceforth referred to as the "slower rate case," and 4.89×10^1 Å/τ, referred to as the "faster rate case." The interaction between the sample and the indenter tip is modeled through a repulsive potential given by[18]

$$U_{\text{ind}}(X_{i,\text{ind}}) = c_i E_0 \exp\left(\frac{\lambda}{H_{\text{ind}}} - \frac{H_{\text{ind}}}{\lambda}\right), \quad X_{i,\text{ind}} < R_{\text{ind}},$$

(16)

where $X_{i,\text{ind}}$ is the distance of site i to the center of the indenter, R_{ind} is the radius of the indenter, $\lambda = R_{\text{ind}} - X_{i,\text{ind}}$, $E_0 = 1$ eV, and $H_{\text{ind}} = 1$ Å. A slab of dimension 10.38 nm $\times$ 5.08 nm $\times$ 10.78 nm containing 46080 sites was used to represent the surface. Periodic boundary conditions were prescribed on four sides parallel to the indentation direction, while the top and the bottom surfaces were kept free.[19] Additionally, a thick layer of sites were held at fixed concentration $c = 0.9999$ around the cell in the direction perpendicular to the indentation direction to serve as vacancy source or sink that correspond to, in reality, climbing dislocations or grain boundaries in the bulk.

During the nanoindentation simulations, several different mechanisms were observed. In the slower rate indentation, surface diffusional creep is evident from the terraced structure shown in Fig. 3(a) that formed spontaneously under the
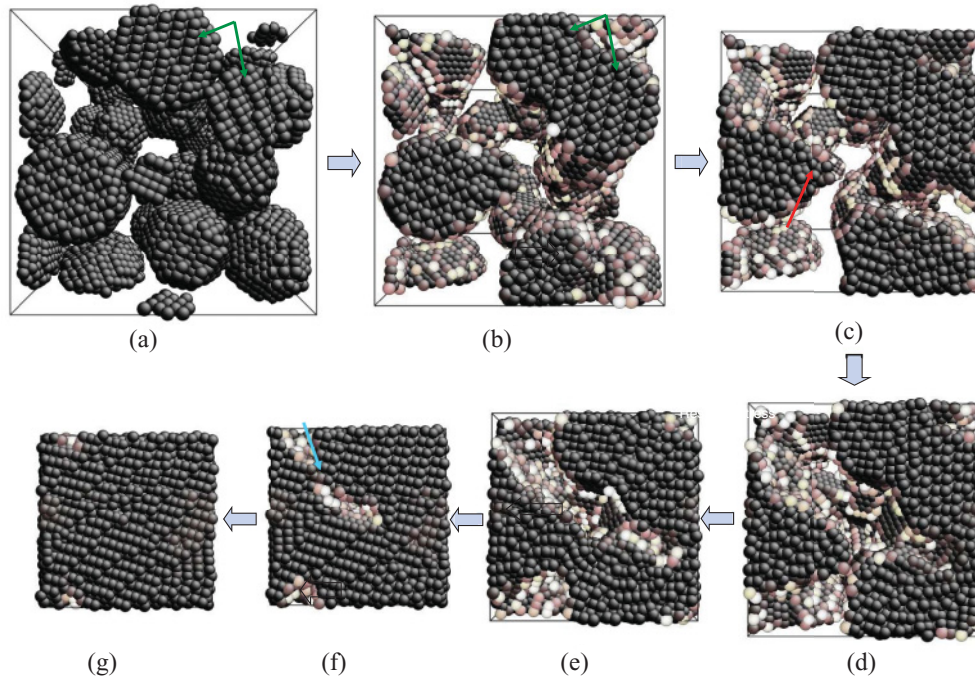
FIG. 5. (Color online) Time evolution of the microstructure at (a) $\tilde{t} = 0$, (b) $\tilde{t} = 1.33$, (c) $\tilde{t} = 4.00$, (d) $\tilde{t} = 6.64$, (e) $\tilde{t} = 9.30$, (f) $\tilde{t} = 12.72$, and (g) $\tilde{t} = 13.30$. Atomic sites with $c \leqslant 0.01$ are not shown. The significance of the arrows is discussed in the text.

indenter before nucleation of any dislocations. No such surface vacancy disk or terrace formed during the faster rate indentation, since diffusion is "frozen" outside of a temperature-strain rate envelope, resulting in a purely Hertzian elastic behavior prior to the onset of displacive plasticity. Figure 3(b) shows the dislocation structure produced after the first large load drop for the slower rate indentation where the surface step provides preferential sites for heterogeneous nucleation of dislocations adjacent to surface defects.[20] This is significantly different from the one observed in the faster rate case, shown in the inset of Fig. 3(b), where dislocation loops were nucleated homogeneously inside the bulk.[21,22] The load-displacement curve [Fig. 3(c)] does show a decrease of the load[23] in the presence of surface diffusion due to diffusional creep accommodation, but the decrease only became large after the mass-deficient defect, i.e., surface vacancy disk, attained a certain size, triggering dislocation nucleation (from surface, not bulk) and subsequent dislocation plasticity, which gave the characteristic serrated flows. These features are qualitatively similar to that of a surface with an initial step observed in experiment[23] and simulation.[20] Our DMD simulations above demonstrate that displacive plasticity can be sensitively controlled by the remnant debris of prior diffusional plasticity.

B. Sintering

To apply DMD to hot isostatic pressing,[24] a simulation cell of dimension $8.80\,\text{nm} \times 8.80\,\text{nm} \times 8.80\,\text{nm}$ containing 24 randomly oriented grains with normally distributed radii [Fig. 4(a)] was chosen with PBC. Empty "ghost" sites with $c = 10^{-4}$, equal to the background vacancy concentration, were added surrounding the grains to allow diffusion into the pore structure for neck formation. The edges of the cell were

compressed down to the theoretical density at a constant rate of $2.25\,\text{Å}/\tau$ at $900\,\text{K}$.

This system represents, to a large extent, the complexity of a realistic situation of many-particle sintering. A movie of this simulation is included in the supplement.[25] In the process of densification, along with surface and grain boundary diffusion, DMD captured mechanical reorientation of particles, plastic deformation, rapid neck formation, consumption of small grains by bigger ones, and breaking of long thin pore structure into pore droplets, in a highly realistic manner. In Figs. 5(a)–5(g), snapshots of the system at different (reduced) times are shown to elucidate some of the above mechanisms. The process of grain rotation and rapid neck formation can be seen in Figs. 5(a) and 5(b) for the particles marked by the green arrows (it happens for many other grains also). The evidence of consumption of smaller grains by bigger ones is shown in Fig. 5(c), indicated by the red arrow. Similarly, by comparing Fig. 5(f) with Fig. 5(e), breaking of the pore into smaller pore structures is evident (cyan arrow). The time evolution of F_{DMD}, as shown in Fig. 4(c) for this closed system, shows a gradual decrease largely due to diffusional processes, occasionally interrupted by sharp reductions as large structural rearrangements are accommodated. These rearrangements occured less frequently at the later stages as it becomes energetically unfavorable for a large grain to rotate. The final configuration [Fig. 4(b)] shows a high degree of homogeneity in structure as well as in chemical potential.

IV. CONCLUSION

In summary, DMD free energy is an atomistic realization of the regular-solution model, with gradient thermodynamics, long-range elastic interactions, and short-range atomic

coordination interactions all included. DMD reveals a microscopic mass-action pathway, which emerges out of the computer simulation automatically while decreasing the free energy, relieving chemical nonequilibrium by short-ranged and long-ranged mass transfer. One view of DMD is that it automatically guides "atom creation" and "atom annihilation" operators in a traditional MD or VG simulation; another equally valid view, coming from the continuum modeling side, is to think of DMD as solving the Cahn-Hilliard equation,[7] but on a moving-atoms grid. Because of the static minimization of $\{\mathbf{X}_i,\alpha_i\}$, the fundamental "clock" of DMD is controlled by the value of diffusivity, not by atomic vibration. Therefore DMD can be seamlessly coupled to continuum diffusion-elasticity field solvers such as finite-element or phase-field method, with adaptive grids down to the atomic scale as in the quasicontinuum method,[26] but now with compositional degrees of freedom as well as the displacive ones.[7]

The present implementations of DMD thermodynamics and kinetics both have errors, though. A more accurate free-energy "density functional" in terms of the site occupations that effectively include pair, triplet, quartet, etc., correlations[27]

could be adopted. The simplistic way of modeling the diffusivity used here does not realistically represent the effect of local environment,[28] deformation, and local stress on kinetics. DMD kinetics is presently just a "downhill ski" on the DMD free-energy landscape, and cannot capture uphill phenomena in mass-action reaction coordinate space due to omission of the noise term. One can, however, easily envision implementing a variety of accelerated dynamics[2,3] and nudged elastic band type calculations[29] with DMD free energy in the extended $\{\mathbf{X}_i,\alpha_i,c_i\}$ space. A future work will address these issues.

For ease of checking, the source code of DMD and input files for all examples in this paper will be placed at a publicly available website.[30]

ACKNOWLEDGMENTS

*liju@seas.upenn.edu

†wang.363@osu.edu

[1] K. R. Elder, M. Katakowski, M. Haataja, and M. Grant, Phys. Rev. Lett. **88**, 245701 (2002).

[2] A. Voter, J. Chem. Phys. **106**, 4665 (1997).

[3] S. Hara and J. Li, Phys. Rev. B **82**, 184114 (2010).

[4] G. Henkelman and H. Jonsson, J. Chem. Phys. **115**, 9657 (2001).

[5] R. LeSar, R. Najafabadi, and D. J. Srolovitz, Phys. Rev. Lett. **63**, 624 (1989).

[6] R. LeSar, R. Najafabadi, and D. Srolovitz, J. Chem. Phys. **94**, 5090 (1991).

[7] Y. Wang and J. Li, Acta Mater. **58**, 1212 (2010).

[8] S. M. Foiles and J. B. Adams, Phys. Rev. B **40**, 5909 (1989).

[9] W. Kohn and L. J. Sham, Phys. Rev. **140**, A1133 (1965).

[10] Y. Mishin, M. J. Mehl, D. A. Papaconstantopoulos, A. F. Voter, and J. D. Kress, Phys. Rev. B **63**, 224106 (2001).

[11] J. Nocedal, Math. Comput. **35**, 773 (1980).

[12] S. Cohen and A. Hindmarsh, Comput. Phys. **10**, 138 (1996).

[13] S. Plimpton, J. Comput. Phys. **117**, 1 (1995).

[14] R. Balluffi, S. Allen, and W. Carter, *Kinetics of Materials*, 1st ed (Wiley Interscience, 2005).

[15] M. Kabir, T. T. Lau, D. Rodney, S. Yip, and K. J. Van Vliet, Phys. Rev. Lett. **105**, 095501 (2010).

[16] D. Setman, E. Schafler, E. Korznikova, and M. J. Zehetbauer, Mater. Sci. Eng. A **493**, 116 (2008).

[17] W. Li and R. Warren, Acta Metall. Mater. **41**, 3065 (1993).

[18] K. J. Van Vliet, J. Li, T. Zhu, S. Yip, and S. Suresh, Phys. Rev. B **67**, 104105 (2003).

[19] Y. Lee, J. Park, S. Kim, S. Jun, and S. Im, Mech. Mater. **37**, 1035 (2005).

[20] J. A. Zimmerman, C. L. Kelchner, P. A. Klein, J. C. Hamilton, and S. M. Foiles, Phys. Rev. Lett. **87**, 165507 (2001).

[21] C. L. Kelchner, S. J. Plimpton, and J. C. Hamilton, Phys. Rev. B **58**, 11085 (1998).

[22] J. Li, K. Van Vliet, T. Zhu, S. Yip, and S. Suresh, Nature (London) **418**, 307 (2002).

[23] J. Kiely, R. Hwang, and J. Houston, Phys. Rev. Lett. **81**, 4424 (1998).

[24] S.-J. L. Kang, *Sintering: Densification, Grain Growth, and Microstructure* (Elsevier, 2005).

[25] See Supplementary Material at http://link.aps.org/supplemental/10.1103/PhysRevB.84.054103 for movie.

[26] E. Tadmor, M. Ortiz, and R. Phillips, Philos. Mag. A **73**, 1529 (1996).

[27] D. de Fontaine, Solid State Phys. **47**, 33 (1994).

[28] A. Van der Ven and G. Ceder, Phys. Rev. Lett. **94**, 045901 (2005).

[29] G. Henkelman, B. P. Uberuaga, and H. Jonsson, J. Chem. Phys. **113**, 9901 (2000).

[30] [http://alum.mit.edu/www/liju99/DMD/].